

# Simulating Cosmic Reionization

Ilian T. Iliev (University of Zürich), Paul R. Shapiro (University of Texas at Austin),  
Garrelt Mellema (University of Stockholm), Hugh Merz (University of Waterloo),  
Ue-Li Pen (Canadian Institute for Theoretical Astrophysics, University of Toronto)

## ABSTRACT

The first billion years of the history of the Universe, commonly referred to as the Cosmic Dark Ages and the Epoch of Reionization, constitute a crucial missing link in our understanding of the evolution of the intergalactic medium and the formation and evolution of galaxies. As gravity gradually amplified the small density contrasts in this dark-matter-dominated universe, structure arose hierarchically, with small objects condensing out first, then merging with each other to make ever larger objects in a clustered pattern in space known as the Cosmic Web. Less than a hundred million years after the Big Bang, the stars forming in the first dwarf galaxies began to release ionizing radiation, which leaked out of these galaxies and caused ionization fronts to sweep outward through the surrounding primordial atomic gas, gradually transforming the cold, neutral intergalactic medium into a hot, ionized one. This epoch of reionization ended before the universe was a billion years old, at a time from which the light now reaching us has its wavelength redshifted by about a factor of 7. Due to the complex nature of this global process it is best studied through large-scale numerical simulations. A number of large observational efforts trying to detect this process directly are currently under way, and their success depends critically upon correctly modelling its observable signatures.

Such simulations present considerable challenges, however, related to the large dynamic range required and the necessity to perform fast and accurate radiative transfer calculations. The hierarchical nature of cosmological structure formation in the Cold Dark Matter paradigm means that, at these early times, the dominant contributors of ionizing radiation were dwarf galaxies of around one billion Solar masses. These tiny galaxies must be resolved in very large cosmological volumes in order to derive their clustering properties and the corresponding observational signatures correctly, which makes this one of the most challenging problems of numerical cosmology.

We have recently performed the largest and most detailed simulations of the formation of early cosmological large-scale structures and their radiative feedback leading to cosmic reionization. This was achieved by running extremely large,  $1728^3$ - to  $3072^3$ -particle (5.2 to 29 billion) N-body simulations of the formation of the Cosmic Web, with enough particles and sufficient force resolution to resolve all the galactic halos with total masses larger than 100 million Solar masses in computational volumes of  $(64/h \text{ Mpc})^3$  to  $(114/h \text{ Mpc})^3$ , respectively. These results were then post-processed by propagating the ionizing radiation from all (up to millions of) sources by using fast and accurate ray-tracing radiative transfer method. For these simulations, we utilized a P<sup>3</sup>M N-body code called CubeP<sup>3</sup>M and a radiative transfer code called C<sup>2</sup>-Ray, both developed by us. Both codes are parallelized using a combination of MPI and OpenMP and to this date have been run efficiently on up to 2048 cores (CubeP<sup>3</sup>M) and up to 10000 cores (C<sup>2</sup>-Ray) on the newly-deployed Sun Constellation Linux Cluster (Ranger) at the Texas Advanced Computing Center.

In this paper we briefly present our codes, methods and parallelization strategies, discuss our recent simulations and results and outline our future plans.

## 1 INTRODUCTION

Reionization is generally believed to be the outcome of the release of ionizing radiation by galaxies undergoing star formation (see for example (1; 2) for recent reviews). Current theory suggests that the galaxies responsible for most of this radiation are dwarf galaxies more massive than about  $10^8 M_\odot$ . In the Cold Dark Matter (CDM) universe nonlinear structures form from initially small-amplitude, Gaussian-random-noise density fluctuations, by a continuous hierarchical sequence of mergers and infall with the smallest galaxies forming first and merging to yield larger ones, forming the Cosmic Web of structures (Fig. 1). While dark matter dominates the gravitational forces which cause this structure formation, ordinary atomic matter must join the dark matter in making galaxies for star formation to be possible. Once the atomic gas in the intergalactic medium (IGM) in some region is heated by reionization, however, gas pressure opposes gravitational collapse, and, thereafter, the smallest galaxies form without atomic matter and cannot make stars. The minimum mass of star forming galaxies in such regions is about one billion solar masses.

Due to the complex nature of the reionization process it is best studied through large-scale numerical simulations (6; 23; 10; 22). Such simulations present considerable challenges related to the large dynamic range required and the necessity to perform fast and accurate radiative transfer calculations. The tiny galaxies which are the dominant contributors of ionizing radiation must be resolved in very large cosmological volumes, large enough to contain billions of times more total mass than one dwarf galaxy and up to tens of millions of such galaxies, in order to correctly derive their numbers and clustering properties. The correct number densities and clustering of these ionizing sources impact strongly the corresponding observational signatures. The ionization fronts expanding from all these millions of galaxies into the surrounding neutral IGM should then be tracked with a 3D radiative transfer method and the full non-equilibrium chemistry should be solved in order to derive the resulting ionization state of the IGM. The combination of all these requirements makes this problem a formidable computational task.

We have recently performed the largest and most detailed simulations of the formation of early cosmological large-scale structures and their radiative feedback leading to cosmic reionization. This was achieved by running extremely large,  $1728^3$ - to  $3072^3$ -particle (5.2 to 29 billion) N-body simulations of the formation of the Cosmic Web, with enough particles and sufficient force resolution to resolve all the galactic halos with total masses larger than 100 million Solar masses in computational volumes of  $(64/h \text{ Mpc})^3$  to  $(114/h \text{ Mpc})^3$ , respectively. These results were then post-processed by propagating the ionizing radiation from all (up to millions of) sources by using fast and accurate ray-tracing radiative transfer method. For these simulations, we uti-

2008.08.27 10:08:06.22877

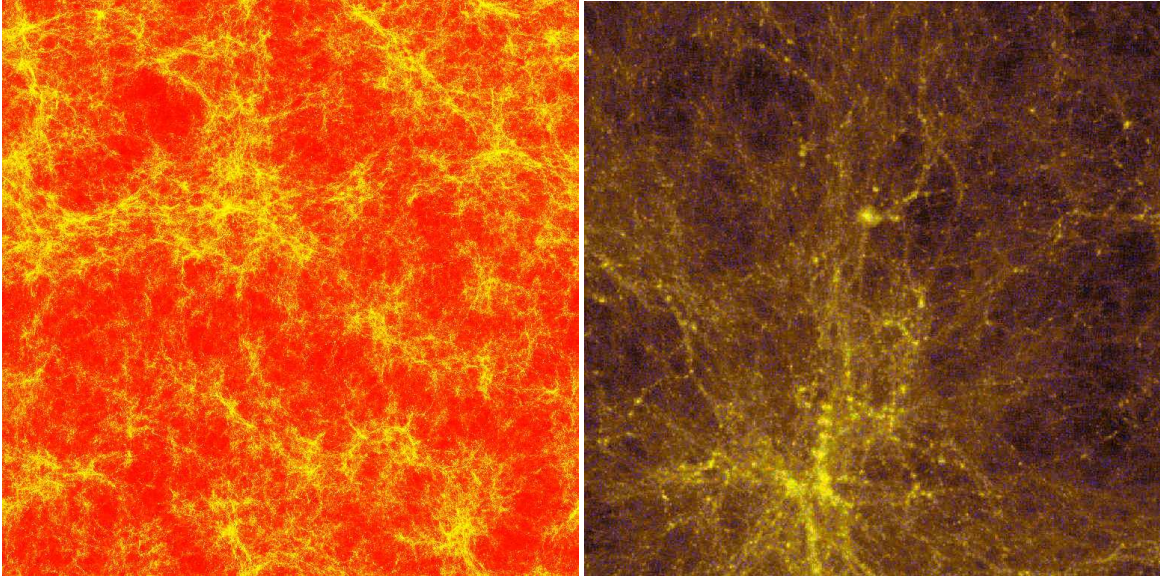


Figure 1: (left) Slice of the Cosmic Web of Dark Matter at redshift  $z = 6$  from our CubeP<sup>3</sup>M Code simulation with  $3072^3$  particles (29 billion) on a  $6144^3$  fine grid in a comoving volume of 163 Mpc on a side. (right) zoom-in of  $10 \text{ Mpc} \times 10 \text{ Mpc}$  subregion. Slices are 20 Mpc thick.

lized a P<sup>3</sup>M N-body code called CubeP<sup>3</sup>M and a radiative transfer code called C<sup>2</sup>-Ray, both developed by us.

Our original simulations of the same process (6) resolved the formation of all galaxies more massive than about one billion solar masses, those which are expected to form stars even after reionization has heated their environment. With this new generation of simulations we explore the role of less massive dwarf galaxies. These are important sources of ionizing radiation if they form before their neighborhood is reionized but are prevented from being sources if they form after it is reionized. Our preliminary results show that the inclusion of these sources and of their suppression changes the outcome of reionization substantially.

## 2 CUBE P<sup>3</sup>M CODE

CubeP<sup>3</sup>M is a massively-parallel P<sup>3</sup>M (particle-particle-particle-mesh) (4) cosmological N-body code written in Fortran 90. It is a successor of the code PMFAST (16) and shares many of its basic characteristics, particularly regarding the treatment of long-range (PM) gravitational forces. Here we briefly describe the code, focusing on the new elements which distinguish it from its predecessor and have not been previously discussed. The main new features are:

- Massive parallelization and scalability to thousands of nodes, using (cubical) domain decomposition.
- Inclusion of short-range direct particle-particle (PP) forces.

The code uses the FFTW 2.1.5 library and MPI-1, as well as (optional) OpenMP threading within each node in order to optimize the memory usage by reducing the amount of buffers necessary for the domain decomposition. CubeP<sup>3</sup>M contains two mesh levels, a coarse and a fine mesh. The mesh sizes per dimension are 2x the number of particles (fine mesh) and half the number of particles (coarse mesh). The superposition of the forces produced by each of these mesh levels, as well as the local particle-particle force, produces the total force on a particle in a given iteration of the code.

The computational domain is decomposed into equal-size cubical sub-regions, which are distributed across the nodes, with a 24-cell

shared buffer zone around each domain. As a consequence of this decomposition CubeP<sup>3</sup>M must be run on an integer-cubed number of MPI nodes. Each cuboid corresponds to the local section of the mesh, which is calculated in parallel by all nodes during each timestep. Since the coarse mesh is 4 times coarser per dimension than the fine mesh (which can be considered as the equivalent 1-level particle-mesh resolution), the total parallel workload is 64x less than the fine mesh simulation volume and does not suffer the performance bottleneck of having to calculate massive distributed FFTs. Each nodal cuboid is then decomposed into a number of fine mesh cuboid tiles for calculating the fine mesh forces. This is done to provide distinct work units for each of the threads on a node to process in parallel through multi-threading, as well as to decrease the amount of memory used to store the arrays associated with the fine mesh gravitational calculation.

We note that our approach of splitting the computational volume into equal-size sub-domains, can in principle result in a work imbalance between nodes and thus diminished efficiency. However, for cosmological simulations of a sufficiently large volume of the Universe this does not pose significant problems, as in practice the variations of particle numbers between the (relatively large) sub-volumes are fairly small. The same would not be true for e.g. detailed simulations of a single dark matter halo. We have thus geared the code to the problem at hand, rather than trying to be universal.

Initial conditions are generated by a separate code using the standard Zel'dovich approximation and primordial power spectrum transfer function given by either the CMBFAST or CAMB Boltzmann code (both publicly available). The main code is then started, with the following algorithmic steps:

- Calculate the timestep for the current iteration, constraining it based on expansion (using the Friedmann equation) and the maximum acceleration components from the previous timestep.
- Update the particle positions using the leapfrog method in half-timestep increments. We actually merge the update from the second half of the previous step with the first half of the current step, as the velocities of the particles do not change
- Construct a linked list for particles within the local volume based on their location within the coarse mesh. This dramatically

speeds up the particle searches which are used in the following steps.

- Pass particles amongst nodes. Particles that move outside of the local physical volume are passed to adjacent nodes, as well as copies of local particles that are required to construct buffer densities. Each dimension is treated independently and done synchronously, reducing the number of communication messages to 6 from a possible 26 neighbors. As each pass is done the particles are added to the linked list.
- Calculate fine mesh accelerations and apply to all particles in the same fashion as PMFAST (16).
- Calculate the particle-particle forces between particles within a fine-mesh grid cell and use the resulting acceleration to update their velocities.
- Calculate the coarse mesh (long-range) accelerations and apply these to all particles in the same fashion as PMFAST. As we use FFTW (3), which only includes a 1-dimensional (slab) decomposition MPI FFT implementation, we have written a wrapper layer that efficiently re-distributes the 3-dimensional (cubical) decomposition data to and from slab decomposition to perform the Fourier space convolution.
- Update the particle positions at the end of the timestep and optionally checkpoint, calculate a density projection, or find halos. There are also options to output the coarse-mesh density, bulk velocity fields, and gas clumping for use in radiative-transfer simulations and to compare with observational predictions.
- If we have reached the final redshift the simulation ends, otherwise we delete particles outside of physical volume and repeat these steps.

The particle-particle force resolution at sub-grid distances is achieved by including approximate direct particle-particle interactions, as follows. An NGP (nearest grid point) force kernel is used to calculate the fine mesh force. This kernel has the property that forces amongst particles within a grid cell are zero, and thus provides the simplest method by which to match the particle-particle forces with the fine mesh forces.

We calculate an additional PP force during fine mesh force velocity update, which allows us to avoid loading the particle list twice and also to thread the operation without any significant additional work. In this routine, all of the particles within a fine mesh tile are read in via the linked list and the appropriate force is applied depending on where they exist within the fine mesh tile. As the linked list chains particles within a coarse mesh cell, for the particle-particle interaction we proceed by constructing a set of fine-cell linked list chains for each coarse cell. We then proceed by calculating the particle-particle force between all particles within a fine mesh cell, limiting pairs to those exceeding a particular softening length (usually set to a twentieth of the initial inter-particle spacing) to prevent scattering. As this proceeds, we also accumulate the PP force applied to each particle and then determine the maximum force applied to a particular particle, which is then used to constrain the length of the global timestep.

The biggest problem with this method is that it is anisotropic and depends on the location of the fine mesh with respect to the particles. An example are two particles on either side of a grid cell boundary. These particles will experience the 1-grid cell separation NGP mesh force, but if the mesh were shifted such that they were within the same cell, they would experience a larger force. We assume that on average this balances out, and we have even tuned the NGP force kernel to provide as unbalanced of a force as possible at grid cell distances

by running large numbers of pairwise force comparisons at different separations and positions relative to the mesh. This effect is even more pronounced at the initial stages of the simulation where the density is more homogeneous, and leads to mesh artifacts appearing in the density field. In order to minimize this effect we have taken to shifting the particle distribution relative to the mesh by a small random amount, up to 2 fine grid cells in magnitude, in each dimension, at each timestep. This adds negligible computational overhead as it can be applied during the particle position update and suppresses this behavior over multiple timesteps.

In the interest of speed and efficiency the halo catalogues are constructed on-the-fly at a pre-determined list of redshifts. We use a spherical over-density (SO) halo finder based on the density distribution on the fine mesh (11). The code first builds the fine-mesh density for each tile. It then proceeds to find and record all local density maxima within the physical volume (excluding buffers) for the tile. It then uses parabolic interpolation on the density field to determine the location of the maximum within the cell, and records the peak position and value. Once the list of maxima is generated they are sorted from highest to lowest. Then each of the halo candidates is inspected independently starting with the highest peak. The grid mass is accumulated in shells surrounding the maximum until the average density of the halo drops below a pre-defined overdensity cutoff (usually set to 178, in accordance with the top-hat collapse model). As we accumulate mass we remove it from the mesh, so that no mass is double-counted. This method is inappropriate for finding sub-halos as those are naturally incorporated in their host halos. After this stage we do another pass through the halo list, this time using the mass measured above to determine the radius of the halo and finding all particles which are within this radius. Those are then used to calculate the halo bulk velocity, internal velocity dispersion and angular momentum components, all of which are listed in the final halo catalogues.

### 3 C<sup>2</sup>-RAY CODE

C<sup>2</sup>-Ray (Conservative Causal Ray-Tracing) is a grid-based ray-tracing radiative transfer and non-equilibrium chemistry code. The method and our algorithm were described in detail in (14). The code is explicitly photon-conserving in both space and time, which ensures correct tracking of ionization fronts without loss of accuracy independent of the spatial and time resolution, with corresponding great gains in efficiency. The code has been tested in detail against a number of exact analytical solutions (14), as well as in direct comparison with a number of other independent radiative transfer methods on a standardized set of benchmark problems (5). There is also a version of the code which is directly coupled to hydrodynamics evolution (13).

The ionizing radiation is ray-traced from every source to every grid cell using a short characteristics method, in which the neutral column density up to a given cell is given by interpolation of the column densities of the previous cells towards the source, in addition to the neutral column density through the cell itself. The contribution of each source to the local photoionization rate of a given cell is first calculated independently, after which all contributions are added together and then non-equilibrium chemistry solver is used to calculate the resulting ionization state. Normally multiple sources contribute to a local photoionization rate. Changes in the rate modify the neutral fraction and thus the neutral column density, which in turn changes the photoionization rates themselves (since either more or less radiation reaches the cell). An iteration procedure is thus called for in order to converge to the correct, self-consistent solution.

The previous version of the code has been used for simulations of cosmic reionization and its observability (e.g. 6; 15; 7; 8; 9) and radiative feedback in turbulent molecular clouds (13). While our basic methodology remains essentially as described in (14), recently the C<sup>2</sup>-

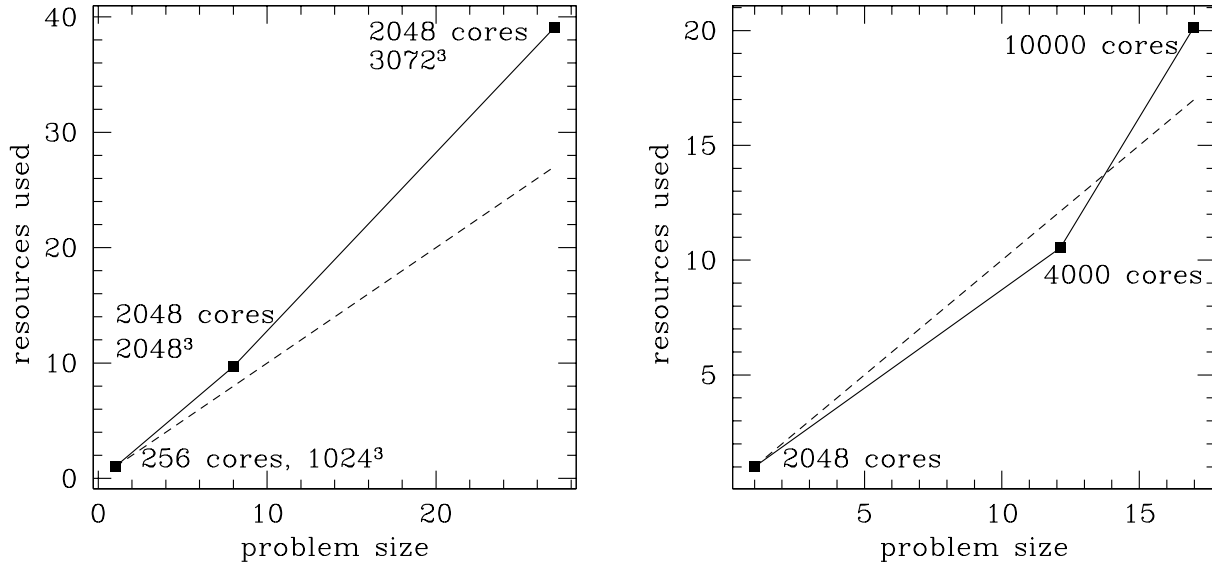


Figure 2: (a)(left) Scaling of the CubeP<sup>3</sup>M code. Plotted are the computational resources used, (wall-clock time)  $\times$  (number of cores) vs. the problem size given by the total number of particles, both quantities normalized to the smallest of the three runs compared. (b)(right) Scaling of the C<sup>2</sup>-Ray code. Plotted are the computational resources used, (wall-clock time)  $\times$  (number of cores) vs. the problem size, (number of sources)  $\times$  (number of cells in grid), both quantities normalized to the smallest of the three runs compared.

Ray has been thoroughly re-written in Fortran 90, made more flexible and modular and parallelized for distributed-memory machines. In terms of parallelization strategy, due to the causal nature of the ray-tracing procedure (i.e. the state of each cell can be calculated only after all previous cells towards the source are done) it is not possible to employ domain decomposition (except for a limited one, into octants, see below), although other approaches exist which seek ways to overcome this limitation (17; 20). Instead, the main code loop over the sources of ionizing radiation is done in massively parallel fashion. Each MPI node has a copy of the density field and receives a number of sources whose radiation to trace through the grid. The sources can be distributed over the nodes either statically, or dynamically, using a master-slave approach, whereby one node distributes the work amongst the rest. The static allocation is preferable for relatively small number of nodes (up to  $\sim 32$ ), while the dynamical approach is better for larger systems. As long as the total number of sources is significantly larger than the number of MPI nodes such parallelization is very efficient. For the large-scale cosmological reionization problem there are typically hundreds of thousands to millions of sources, thus our code scales well up to tens of thousands of cores (see next section). For problems with a (relatively) low number of ionizing sources such a parallelization strategy would be inefficient, but such problems are not sufficiently computationally-intensive to require massive parallelization and could, instead, be solved on a smaller number of nodes, or even in serial. A similar situation occurs for the initial steps of the simulations presented below, when the cosmological structure formation is not yet much advanced, thus only a few to tens of halos form. However, their number increases exponentially with time, quickly reaching thousands, and then tens and hundreds of thousands. We therefore start our simulations on a small number of cores (typically 32), and increase this number as more sources form. Since the current version of the code requires that a complete copy of the grid is available on each node, it has relatively high memory-per-node requirements. E.g. a  $432^3$  mesh requires  $\sim 6.6$  GB per node to run. Therefore, Ranger, with its large amounts of RAM available per node is a perfect platform for high-resolution radiative transfer runs.

As mentioned above, a limited domain decomposition into octants is possible for our method, since those are independent of each other within the short-characteristic ray-tracing framework. We use this to (optionally) improve the memory efficiency of the code by doing the grid octants in parallel within each MPI node using OpenMP multithreading. This way each MPI node needs only one copy of the grid, which is shared amongst the cores within the node.

#### 4 SIMULATIONS AND SCALING

We have conducted a series of N-body structure formation simulations, with particle numbers of  $1024^3$ ,  $1500^3$ ,  $1728^3$ ,  $2048^3$  and  $3072^3$  and box sizes of 53 Mpc, 80 Mpc, 91 Mpc, 103 Mpc and 163 Mpc, respectively<sup>1</sup>. At earlier times the physical volume will be smaller by a factor  $1/(1+z)$ . The last in this series is the largest simulation of the formation of early cosmological structures done to date. The  $1500^3$  and  $1728^3$ -particle simulations were ran on the Dell Linux Cluster (Lonestar) at TACC on 500 and 432 cores, respectively, while the  $1024^3$ ,  $2048^3$  and  $3072^3$  were ran on the newly-deployed Sun Constellation Linux Cluster (Ranger) at TACC, on 256, 2048 and 2048 cores, respectively. The latter three simulations were ran with 4 MPI processes and 4 threads per node (using the *tacc\_affinity* script to ensure local memory affinity) and required 4,100, 40,000 and 159,000 SUs (cores  $\times$  hours).

All simulations use the same particle mass,  $5 \times 10^6 M_\odot$ . This mass resolution allows us to resolve, with 20 particles or better, all halos with a mass above  $10^8 M_\odot$ . This mass roughly corresponds to a halo virial temperature of  $10^4$  K, and thus is the minimum halo mass for the gas in the halo to be able to cool through hydrogen atomic-line cooling and efficiently form stars. Gas in halos smaller than that can only cool through molecular, as well as metal-line cooling, which is less efficient since molecules get destroyed relatively easily, while metals (elements heavier than He) are not present in significant amounts so early in the history of the Universe. The halos are divided further into halos with

<sup>1</sup>These box sizes denote the so-called comoving size, i.e. the physical size this volume will have at redshift 0 (the current time).

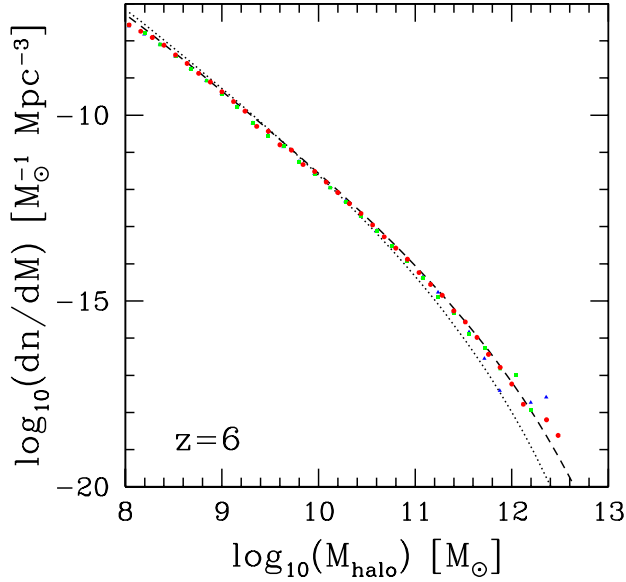


Figure 3: Mass functions at  $z = 6$  from the N-body simulations with box sizes 91 Mpc (blue triangles), 103 Mpc (green squares) and 163 Mpc (red circles). All three mass functions demonstrate excellent agreement, except for the largest halos which are subject to cosmic variance for the smaller volume simulations. The lines show the predicted mass functions based on the well-known analytical models of Press-Schechter ((18); dotted) and Sheth-Tormen ((21); dashed).

mass above the Jeans mass of the ionized and heated medium (roughly above  $10^9 M_\odot$ ), which are not affected by reionization and lower-mass halos, whose star formation is suppressed in ionized regions.

Based on the results from the N-body simulations, i.e. the halo catalogues and density field (re-gridded to a coarser grid), we run our radiative transfer reionization simulations. Our methodology for these simulations is described in detail in (6; 15; 7). In short, all halos are assumed to host galaxies (thus, ionizing sources), to which we assign ionizing photon luminosity proportional to the halo mass, with an efficiency  $f_\gamma$ , giving the number of photons emitted per atom over the lifetime of the source (here assumed to be 11.5 Myr). The simulations are denoted f100\_250S\_91Mpc\_216, f100\_250S\_91Mpc\_432 and f50\_250S\_163Mpc\_384, where the first two numbers are the values of  $f_\gamma$  for the high- and low-mass sources (“S” is for source suppression due to Jeans-mass filtering, the third is the box size and the last is the radiative transfer grid resolution per dimension. The first two simulations are currently finished, while the last (and largest) is still running. All three simulations ran on Ranger with 4 MPI processes and 4 threads per node and took approximately 90,000, 700,000 and (to date) 500,000 SUs, respectively.

Both CubeP<sup>3</sup>M and C<sup>2</sup>-Ray are designed for weak scaling, i.e. if the number of cores and the problem size increase proportionally to each other, for ideal scaling the wall-clock time should remain the same, in contrast to “strong” scaling, whereby the same problem solved on more cores should take proportionally less wall-clock time. This weak scaling requirement is dictated by the problems we are trying to solve (very large and computationally-intensive) and our aims, which are to do such large problems efficiently, rather than for the least wall-clock time. Some scaling results are shown in Fig. 2.

For the N-body simulations we concentrate on the three Ranger runs, so as to eliminate the complicating factor of comparing different machines, clock speeds, etc. On the horizontal axis we show the size of the problem (defined here as total number of particles, since all three simulations have the same resolution), scaled to the smallest one, while

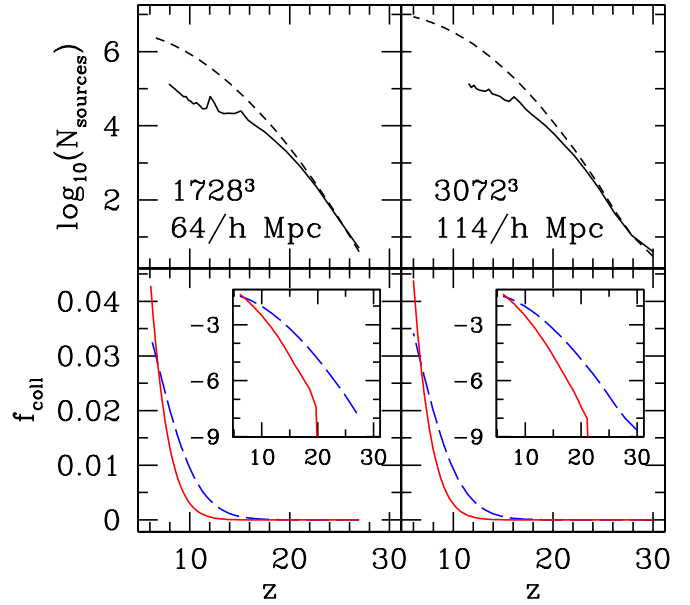


Figure 4: (top panels) Total number of sources (dashed) and number of active sources (i.e. all sources less the suppressed ones; solid); and (bottom panels) collapsed fraction in high-mass (red, solid) and low-mass sources (blue, dashed) (insets show the same in log scale) vs. cosmic redshift for simulations f100\_250S\_91Mpc (left) and f50\_250S\_163Mpc (right).

the vertical axis shows the resources used (SUs) for the complete simulation (evolution from redshift  $z = 300$  to  $z = 6$ ). The code scaling from 256 to 2048 cores and  $1024^3$  to  $2048^3$  particles is excellent, within 20% of the perfect one (dashed line). We expect that this small difference is mostly due to the larger communication overhead for the larger simulation. The largest simulation ( $3072^3$  particles on 2048 cores) differs from the perfect scaling by approximately 40%, demonstrating the strong effect of the communication and I/O overheads (since the number of cores for the  $2048^3$  and  $3072^3$  simulations is the same, the only difference is the larger amount of data that has to be communicated and read/written). The code performance is thus quite satisfactory and it could be expected to scale well to even larger number of cores.

The radiative transfer problem size scales proportionally to both the grid size and the number of sources. In this case we compare the code performance over a single timestep, at  $z \sim 12$ . There are 40,797, 61,840, and 123,257 ionizing sources for the cases f100\_250S\_91Mpc\_216, f100\_250S\_91Mpc\_432 and f50\_250S\_163Mpc\_384, respectively. Results show almost perfect scaling, within  $\sim 15\%$  from the ideal one, for up to 10,000 cores. In fact, the scaling from 2048 to 4000 cores is even slightly better than the “perfect” one, which reflects the fact that the fixed component of the code, is a larger fraction of the total work for a smaller grid (here  $216^3$  vs.  $432^3$ ). On the other hand, our largest run, on 10,000 cores, scales slightly worse, partly due to the same grid effect, but in reverse (the grid is  $384^3$  vs.  $432^3$ ), and partly due to the higher communication overhead in this case.

## 5 RESULTS AND FUTURE WORK

The simulations presented here are still being analysed, but some preliminary scientific results are shown in Figs. 3-5. In Fig. 3 we show the halo mass functions at  $z = 6$  for three of our N-body simulations. All three mass functions are in excellent agreement with each other, except for some (expected) scatter for the largest, rarest halos, which are subject to cosmic variance, particularly for the smaller boxes. The numeri-

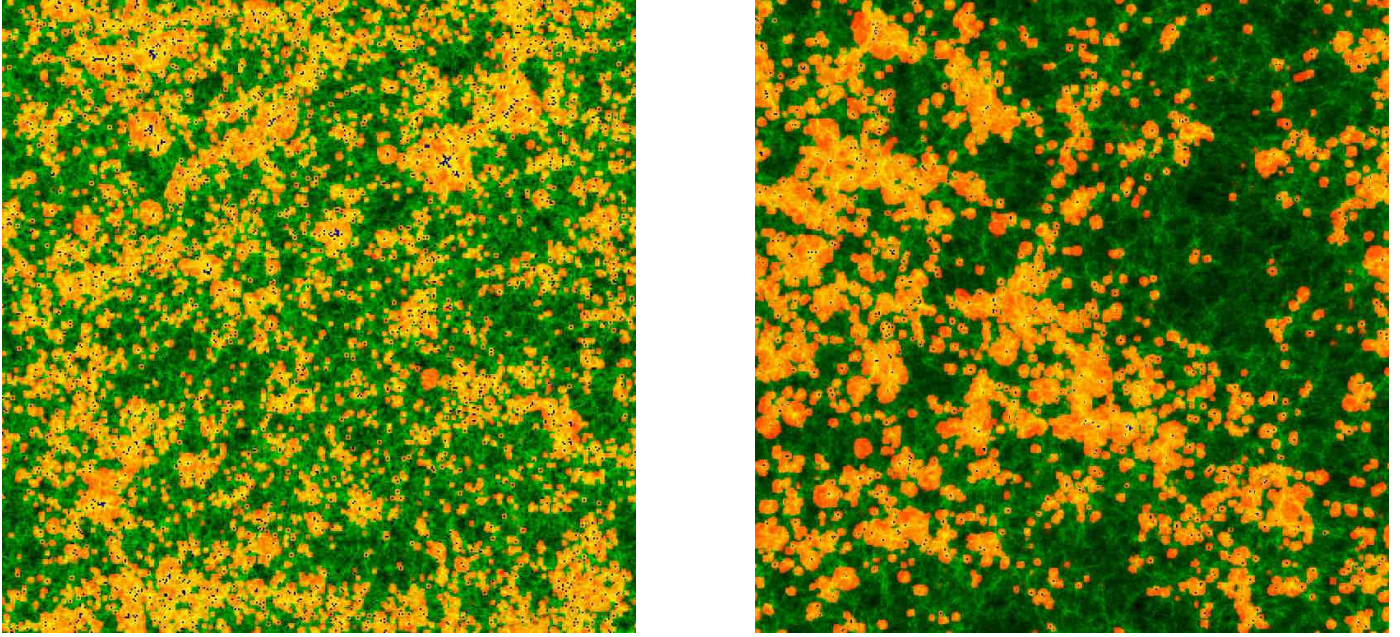


Figure 5: Spatial slices of the ionized and neutral gas density from our radiative transfer simulations (a)(left) boxsize 163 Mpc at redshift  $z = 11.6$  and (b)(right) boxsize 91 Mpc at  $z = 11.9$ , both at ionized fraction by mass  $x_m = 0.30$ . Shown are the density field (green) overlaid with the ionized fraction (red/orange/yellow) and the cells containing sources (dark/blue). There is a good agreement between the two simulations in the typical sizes of the locally-percolated ionization bubbles. The slice thickness is  $1/h$  Mpc for the 64/h Mpc box and  $0.3/h$  Mpc (1 cell) for the 114/h Mpc box. The sources are projected from thicker slices:  $1/h$  Mpc for the 64/h Mpc box and  $3.3/h$  Mpc for the 114/h Mpc box.

cal results are in good agreement with the analytically-predicted Sheth-Tormen mass function (21), but not with the Press-Schechter one (18), which strongly under-predicts the abundances of the rare halos and over-predicts the abundances of the low-mass ones (also see (6; 19; 12)). In Fig. 4 we show the evolution of the total source numbers, active source numbers and collapsed fractions (i.e. the fraction of the total mass found in sources) for the two types of sources. The collapsed fractions from the two simulations agree to within a few percent (relative) and the halo numbers show a similar agreement (once the different simulation volumes are taken into account). The biggest difference is found at very early times, when only a few, rare sources have formed, which are subject to strong cosmic variance. E.g. for the 163 Mpc box the first halos form already at redshift  $z \sim 30$ , while for 91 Mpc the first sources only form at  $z \sim 27$ , due to the 5.6 times smaller volume which is simulated and, more subtly, due to the inevitable cutoff at the box size of longest-wavelength density perturbation modes, which changes the statistics and bias of the rarest halos.

Finally, in Fig. 5 we show some images of the density field and (active) source distribution overlaid with the ionized fraction derived from our radiative transfer simulations. These indicate the very complex and evolving geometry and topology of the network of ionized bubbles and neutral patches, which needs to be studied in detail in order to make predictions for the many observational experiments aiming to detect these remote epochs.

We have planned and are working on a number of improvements of the codes and the simulations presented here. A very important development will be to directly couple the CubeP<sup>3</sup>M and C<sup>2</sup>-Ray codes, which will allow us to run simulations of the feedback of radiation on the gas in the forming cosmic structures. Such feedback is particularly important at small spatial scales and can modify significantly the forming structures, with corresponding observational implications. There are some significant issues to overcome in terms of the efficient parallelization of such coupled code, due to the very different approaches currently employed for their parallelization, discussed above.

An improvement for CubeP<sup>3</sup>M would be extending the accuracy of

the N-body PP force resolution to multi-grid cell distances. This would dramatically improve the force resolution and further minimize the force anisotropy by allowing the matching to take place at larger separations where the magnitude of the gravitational force is weaker. While this would slow down the calculation, it would help to improve the code efficiency (by increasing the number of calculations while keeping the same amount of communication).

We are also working on improving our halo finding procedure. The current grid-based scheme works quite well for finding and determining the properties of the larger halos (containing 40-50 particles or more), but is somewhat less precise for the smallest halos (down to 20 particles). Our new halo finding method will be independent of the grid and thus more reliable for identifying the smallest halos.

Finally, we also plan to run much larger N-body simulations, with somewhat different scientific goals. The largest of our current simulations, with 29 billion particles, only used  $\sim 3\%$  of the available cores and memory on Ranger. It is entirely within the machine and code specifications to run simulations with up to 165 billion particles (on 10,976 cores) in the near future. Even simulations with over 300 billion particles are in principle possible, provided some current technical issues are resolved. Such extremely large structure formation simulations will be of great value for galaxy survey science since it becomes possible to simulate the whole observable Universe ( $\sim (3h^{-1}\text{Gpc})^3$  volume) in a single simulation with sufficient resolution to identify the typical galaxies seen in large surveys (with luminosity  $L_*$ , roughly similar to our Milky Way Galaxy, or less).

#### ACKNOWLEDGEMENTS

This work was supported in part by Swiss National Science Foundation grant 200021-116696/1, the Swedish Research Council grant 60336701, as well as by NSF grant AST 0708176, NASA grants NNX07AH09G and NNG04G177G, and Chandra grant SAO TM8-9009X.

## REFERENCES

- [1] R. Barkana. The First Stars in the Universe and Cosmic Reionization. *Science*, 313:931–934, August 2006.
- [2] B. Ciardi and A. Ferrara. The First Cosmic Structures and Their Effects. *Space Science Reviews*, 116:625–705, February 2005.
- [3] M. Frigo and S. G. Johnson. The design and implementation of FFTW3. *Proceedings of the IEEE*, 93(2):216–231, 2005. special issue on “Program Generation, Optimization, and Platform Adaptation”.
- [4] R. W. Hockney and J. W. Eastwood. *Computer simulation using particles*. Adam Hilger Ltd., Bristol, UK, 1988.
- [5] I. T. Iliev, B. Ciardi, M. A. Alvarez, A. Maselli, A. Ferrara, N. Y. Gnedin, G. Mellema, T. Nakamoto, M. L. Norman, A. O. Razoumov, E.-J. Rijkhorst, J. Ritzerveld, P. R. Shapiro, H. Susa, M. Umemura, and D. J. Whalen. Cosmological radiative transfer codes comparison project - I. The static density field tests. *MNRAS*, 371:1057–1086, September 2006.
- [6] I. T. Iliev, G. Mellema, U.-L. Pen, H. Merz, P. R. Shapiro, and M. A. Alvarez. Simulating cosmic reionization at large scales - I. The geometry of reionization. *MNRAS*, 369:1625–1638, July 2006.
- [7] I. T. Iliev, G. Mellema, P. R. Shapiro, and U.-L. Pen. Self-regulated reionization. *MNRAS*, 376:534–548, April 2007.
- [8] I. T. Iliev, U.-L. Pen, J. R. Bond, G. Mellema, and P. R. Shapiro. The Kinetic Sunyaev-Zel’dovich Effect from Radiative Transfer Simulations of Patchy Reionization. *ApJ*, 660:933–944, May 2007.
- [9] I. T. Iliev, P. R. Shapiro, P. McDonald, G. Mellema, and U.-L. Pen. Effect of the intergalactic environment on the observability of Ly-alpha emitters during reionization. *ArXiv e-prints*, 711(2944), November 2007.
- [10] K. Kohler, N. Y. Gnedin, and A. J. S. Hamilton. Large-Scale Simulations of Reionization. *ApJ*, 657:15–29, March 2007.
- [11] C. Lacey and S. Cole. Merger Rates in Hierarchical Models of Galaxy Formation - Part Two - Comparison with N-Body Simulations. *MNRAS*, 271:676–+, December 1994.
- [12] Z. Lukić, K. Heitmann, S. Habib, S. Bashinsky, and P. M. Ricker. The Halo Mass Function: High-Redshift Evolution and Universality. *ApJ*, 671:1160–1181, December 2007.
- [13] G. Mellema, S. J. Arthur, W. J. Henney, I. T. Iliev, and P. R. Shapiro. Dynamical H II Region Evolution in Turbulent Molecular Clouds. *ApJ*, 647:397–403, August 2006.
- [14] G. Mellema, I. T. Iliev, M. A. Alvarez, and P. R. Shapiro.  $C^2$ -ray: A new method for photon-conserving transport of ionizing radiation. *New Astronomy*, 11:374–395, March 2006.
- [15] G. Mellema, I. T. Iliev, U.-L. Pen, and P. R. Shapiro. Simulating cosmic reionization at large scales - II. The 21-cm emission features and statistical signals. *MNRAS*, 372:679–692, October 2006.
- [16] H. Merz, U.-L. Pen, and H. Trac. Towards optimal parallel PM N-body codes: PMFAST. *New Astronomy*, 10:393–407, April 2005.
- [17] T. Nakamoto, M. Umemura, and H. Susa. The effects of radiative transfer on the reionization of an inhomogeneous universe. *MNRAS*, 321:593–604, March 2001.
- [18] W. H. Press and P. Schechter. Formation of Galaxies and Clusters of Galaxies by Self-Similar Gravitational Condensation. *ApJ*, 187:425–438, February 1974.
- [19] D. S. Reed, R. Bower, C. S. Frenk, A. Jenkins, and T. Theuns. The halo mass function from the dark ages through the present day. *MNRAS*, 374:2–15, January 2007.
- [20] E.-J. Rijkhorst, T. Plewa, A. Dubey, and G. Mellema. Hybrid characteristics: 3D radiative transfer for parallel adaptive mesh refinement hydrodynamics. *A&A*, 452:907–920, June 2006.
- [21] R. K. Sheth and G. Tormen. An excursion set model of hierarchical clustering: ellipsoidal collapse and the moving barrier. *MNRAS*, 329:61–75, January 2002.
- [22] H. Trac and R. Cen. Radiative Transfer Simulations of Cosmic Reionization. I. Methodology and Initial Results. *ApJ*, 671:1–13, December 2007.
- [23] O. Zahn, A. Lidz, M. McQuinn, S. Dutta, L. Hernquist, M. Zaldarriaga, and S. R. Furlanetto. Simulations and Analytic Calculations of Bubble Growth during Hydrogen Reionization. *ApJ*, 654:12–26, January 2007.